SUPPORTING INFORMATION

for

Surface States Mediate Triplet Energy Transfer in Nanocrystal-Acene Composite Systems

Jon A. Bender,[‡1] Emily K. Raulerson,[‡1] Xin Li,[2] Tamar Goldzak,[3] Pan Xia,[4] Troy Van Voorhis,[3]

Ming Lee Tang,[2,4] & Sean T. Roberts[*1]

[1]*Department of Chemistry, The University of Texas at Austin, Austin, TX 78712*

[2]*Department of Chemistry, University of California Riverside, Riverside, CA 92521*

[3]*Department of Chemistry, Massachusetts Institute of Technology, Cambridge, MA 02139*

[4]*Materials Science & Engineering Program, University of California Riverside, Riverside, CA 92521*

[‡] These two authors contributed equally to this manuscript.

[*] Author to whom correspondence should be sent: roberts@cm.utexas.edu

S1. Synthesis of 2-CP (4-(6,13-bis(2-(triisopropylsilyl)ethynyl)pentacen-2-yl)benzoic acid)

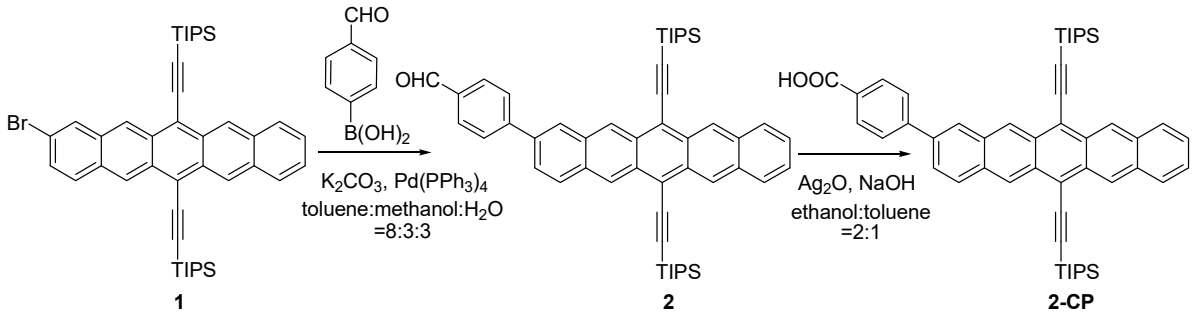

Scheme S1: Synthesis of 2-CP

Compound 1 was synthesized and purified according to procedures published by Sanders et al.[1]

Compound 2 was synthesized and purified following a modified method by Shi et al.[2] **Compound 1** (500 mg, 0.729 mmol), 4-formylphenylboronic acid (136.6 mg, 0.91 mmol), K_2CO_3 (353.0 mg, 2.55 mmol) and 6 mL of toluene: CH_3OH: H_2O =8:3:3 was mixed in a flask. The solution was degassed under argon for 20 min and $Pd(PPh_3)_4$ (22.0 mg, 0.02 mmol, 2.6 mol%) was added under high argon flow. The reaction was then stirred under argon for 6 h at 80 °C. After the mixture was cooled to room temperature, it was extracted with dichloromethane and washed with H_2O several times. The organic layer was then dried with $MgSO_4$, and the solvent was removed with a rotary evaporator. The resulting crude product was purified by silica gel column chromatography and CH_2Cl_2:hexane = 1:1 as the eluent. A blue solid was obtained as the final target (477.9 mg, 88% yield). HRMS (+ESI/ APCI) (mass m/z): 743.4266 $[M+H]^+$. ^1H NMR (400 MHz, $CDCl_3$): δ_H = 10.11 (s, 1H), 9.36 (s, 1H), 9.32 (s, 1H), 9.31 (s, 1H), 9.30 (s, 1H), 8.18 (s, 1H), 8.08 (d, J = 9.1 Hz, 1H), 8.03 (d, J = 8.4 Hz, 2H), 7.98 (m, 2H), 7.94 (d, J = 8.2 Hz, 2H), 7.70 (dd, J = 8.9, 1.5 Hz, 1H), 7.43 (m, 2H), 1.39 (m, 42H) ppm. ^{13}C NMR (400 MHz, $CDCl_3$): δ_C = 191.83, 146.75, 136.80, 135.51, 135.37, 132.40, 132.03, 131.44, 130.91, 130.77, 130.71, 130.41, 129.80, 128.66, 128.02, 127.74, 127.21, 127.16, 126.63, 126.38, 126.35, 126.36, 126.17, 125.56,

118.57, 118.50, 107.56, 107.42, 104.54, 104.52, 19.01, 11.68 ppm.

2-CP was synthesized and purified following a modified method from Shu et al.[3] NaOH (1.41 g, 35.2 mmol) was suspended in ethanol (29 mL) followed by the addition of Ag_2O powder (1.48g, 6.41 mmol). Then **compound 2** (477 mg, 0.628 mmol), dissolved in toluene (14 mL), was added to the suspension. The reaction was kept under argon and allowed to proceed at room temperature for 2 hours. After quenching by careful addition of 10% H_2SO_4, the reaction mixture was extracted with Et_2O. The organic phase was then dried over $MgSO_4$ and concentrated in vacuo to afford a crude acid as a blue solid. The crude solid was then purified by passing through a flash column. A greenish blue solid was obtained as the target (385.7 mg, 91% yield). HRMS (+ESI/ APCI) (mass m/z): 759.4105 $[M+H]^+$. ^{1}H NMR (400 MHz, $CDCl_3$): δ_H = 9.37 (s, 1H), 9.33 (s, 1H), 9.32 (s, 1H), 9.31 (s, 1H), 8.25 (d, J = 8.4 Hz, 2H), 8.19 (s, 1H), 8.08 (d, J = 9.3 Hz, 1H), 7.97 (m, 2H), 7.90 (d, J = 8.2 Hz, 2H), 7.72 (dd, J = 8.9, 1.7, 1H), 7.42 (m, 2H), 1.39 (m, 42H) ppm. ^{13}C NMR (400 MHz, $CDCl_3$): 166.75, 143.24, 136.29, 131.20, 131.05, 130.35, 129.50, 129.43, 129.33, 129.25, 129.12, 128.44, 127.40, 125.86, 125.66, 125.54, 125.43, 125.24, 125.22, 125.15, 125.10, 125.09, 125.02, 124.90, 124.81, 117.12, 117.02, 106.74, 106.59, 103.09, 17.88, 10.39 ppm.

SII. Extraction of Kinetic Rate Constants from Transient Absorption Spectra

To identify timescales for individual steps involved in energy transfer from PbS nanocrystals (NCs) to 2-CP, transient absorption (TA) spectra were fit using a linear decomposition model.[4–6] Briefly, this model assumes TA spectra can be decomposed as:

$$S(\lambda, t) = \sum_n c_n(t)\sigma_n(\lambda). \quad (S1)$$

wherein the time-dependent TA signal, $S(\lambda, t)$, is represented by the sum of a set of time-independent decay associated difference spectra (DADS), $\{\sigma_n(\lambda)\}$, with time-varying amplitudes,

$\{c_n(t)\}$. Each DADS represents the TA spectrum associated with a given excited configuration of the system and contain positive features due to excited state absorption and negative features due to ground state depletion and stimulated emission. For systems with multiple chromophores, such as the 2-CP functionalized PbS NCs (2-CP:PbS) we examine here, DADS can contain contributions from each chromophore.

The amplitude, $c_i(t)$, represents the fraction of the excited population that, at time t, adopts the configuration described by the DADS σ_i. To solve for these coefficients as a function of time, we assume interconversion between different DADS occurs via a series of sequential first-order processes:

$$\begin{aligned} \frac{dc_1}{dt} &= I(t) - k_1 c_1(t) \\ \frac{dc_i}{dt} &= k_{i-1} c_{i-1}(t) - k_i c_i(t). \end{aligned} \qquad (S2)$$

In Eq. S2, the growth of the first DADS is described by $I(t)$, which is taken to reflect the instrument response function for the TA dataset. In modeling TA spectra of 2-CP:PbS measured with femtosecond time resolution, three DADS were found to be sufficient to reproduce dynamics observed throughout the dataset. These spectra appear in Figure 5A of the main text. For completeness, in Figure S1 we compare the fit produced by our model against our experimental data. In practice, to fit this data, an additional DADS was included in the pump-probe overlap region to describe the decay of a coherence spike associated with the nonlinear response of the solvent. Overall, the agreement between the fit and experiment is quite good, thereby allowing us to assign interpretations to the kinetic rates extracted from the model (see main text).

To model dynamics measured in nanosecond time-resolution TA experiments (Figure 4, main text), two DADS were needed that interconvert with a 113-ns time constant. The former of these two DADS we assign to charge carriers localized at PbS surface states while the latter we

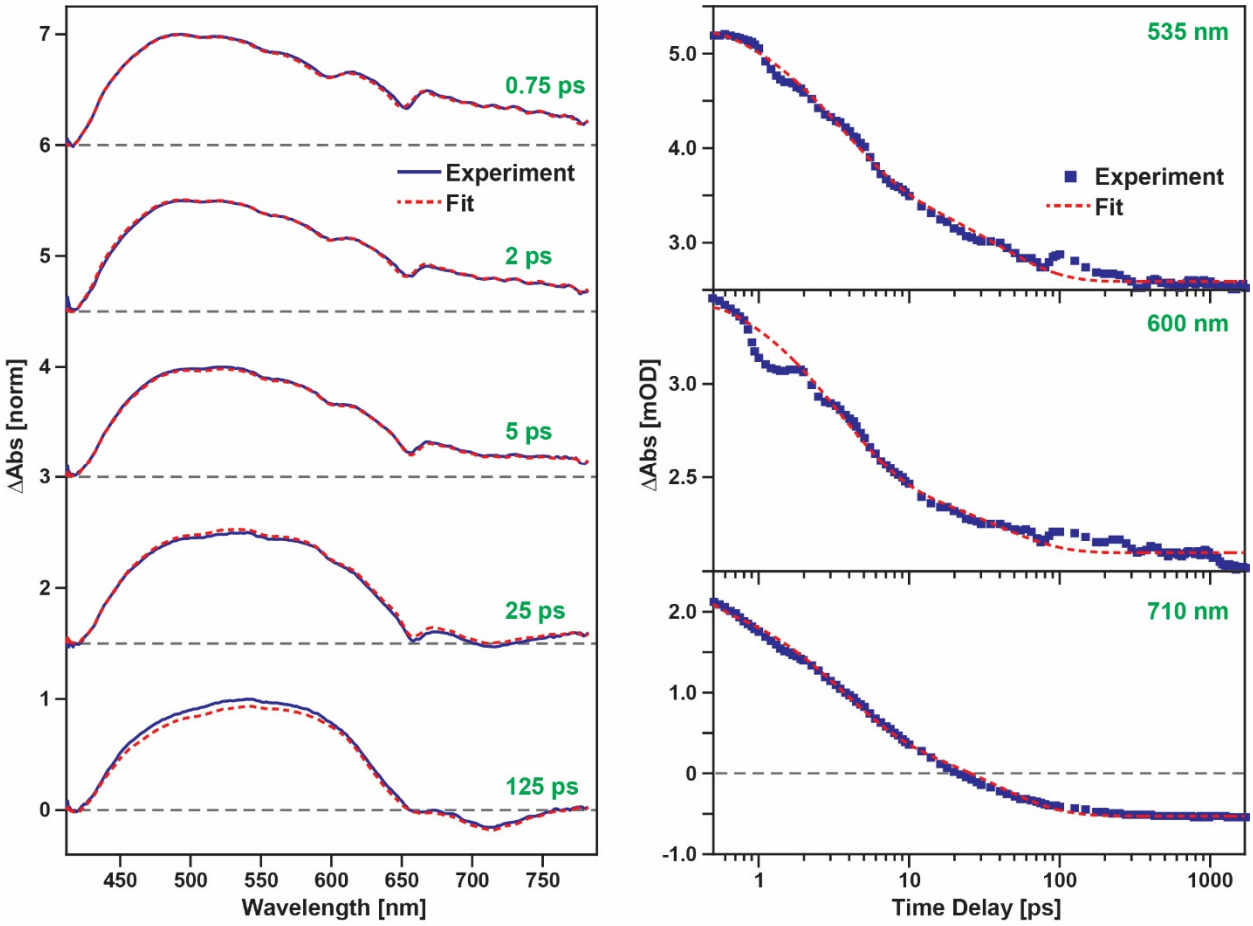

Figure S1: Comparison of 2-CP:PbS TA spectra measured over picosecond time delays (blue) and a fit produced by the linear decomposition model (red dashed). Three DADS were necessary to reproduce changes in the 2-CP bleaching profile and the growth of a new photobleach at 710 nm. Timescales for interconversion between the DADS were found to be 3.3 and 37 ps as described in the main text. Note, each experimental trace in the left column has been normalized to its maximum amplitude for ease of comparison.

attribute to 2-CP triplet excitons. Figure S2 compares experimental TA spectra measured over nanosecond-to-microsecond delays and the fit reconstructed by our model. Similar to data measured with femtosecond time resolution, we include an additional DADS in our model to account for a nonresonant solvent response that decays with the instrument response function. We find our fit model does an accurate job reproducing dynamics measured over nanosecond-to-microsecond time delays. Following their creation, PbS triplet excitons are found to decay to the ground state with a time constant of 1.7 μs.

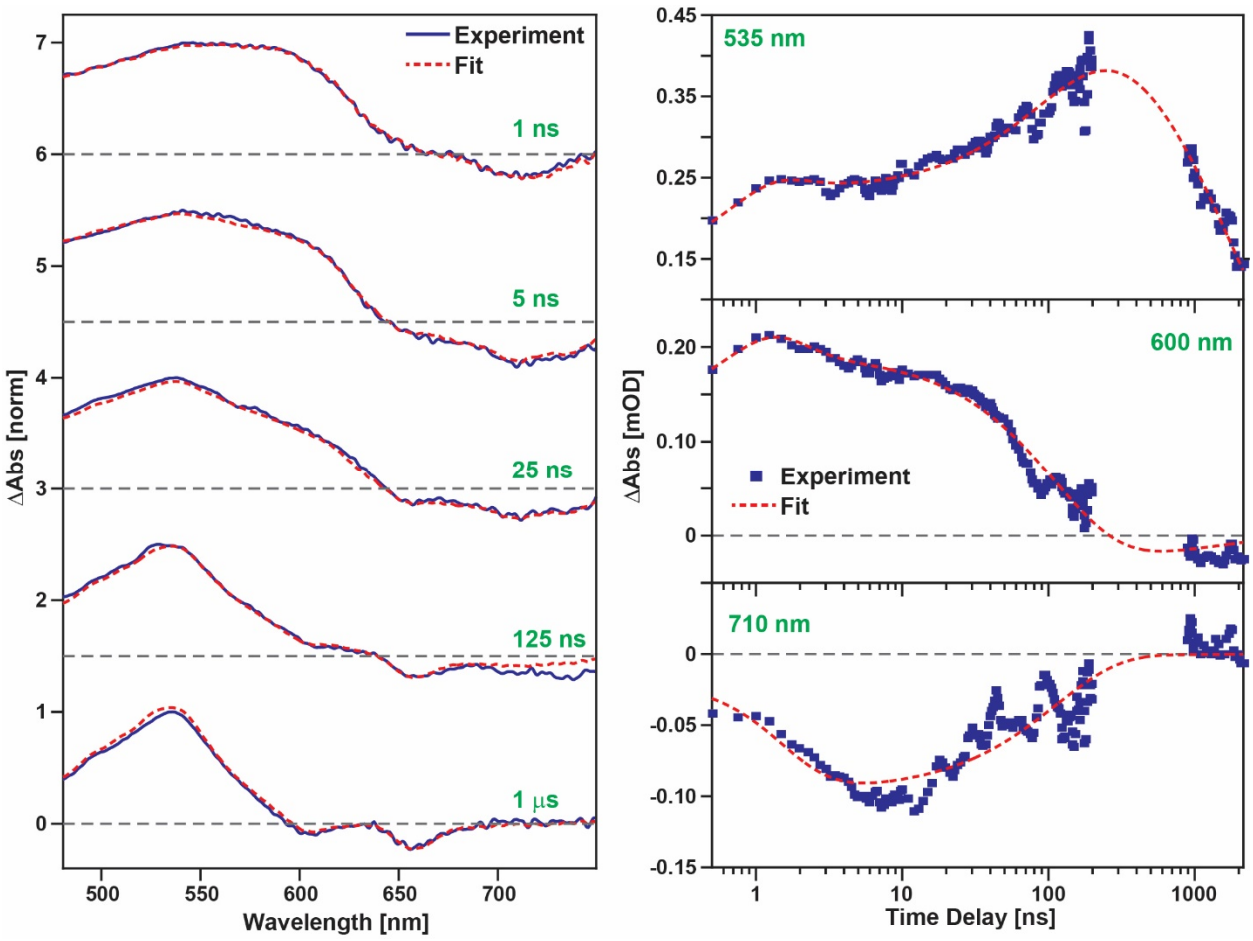

Figure S2: Comparison of 2-CP:PbS TA spectra measured over nanosecond time delays (blue) and a fit produced by the linear decomposition model (red dashed). Two DADS with an interconversion timescale of 113 ns capture the growth of a new induced absorption band near 535 nm and photobleaches at 607 and 657 nm. We assign the growth of these features to the formation of 2-CP triplet excitons based on their similarity to those appearing in triplet sensitization measurements (see Section SVI below). An additional kinetic timescale describing decay of the 2-CP triplet exciton to the ground state (1.7 μs) is included in the fit. Note, each experimental trace in the left column has been normalized to its maximum amplitude for ease of comparison. The gap in the dataset between ~0.25 and 1 μs results from a RF-background that interferes with our detection electronics.

SIII. Stark-Induced Shifts of 2-CP Absorption Transitions

Figure 5 of the main text displays DADS extracted for 2-CP:PbS within the first nanosecond following photoexcitation at 800 nm. Upon photoexcitation, photobleaching features can be seen that are indicative of 2-CP molecules. In the main text, we note the changes we observe immediately following photoexcitation resemble the second derivative of 2-CP's ground state

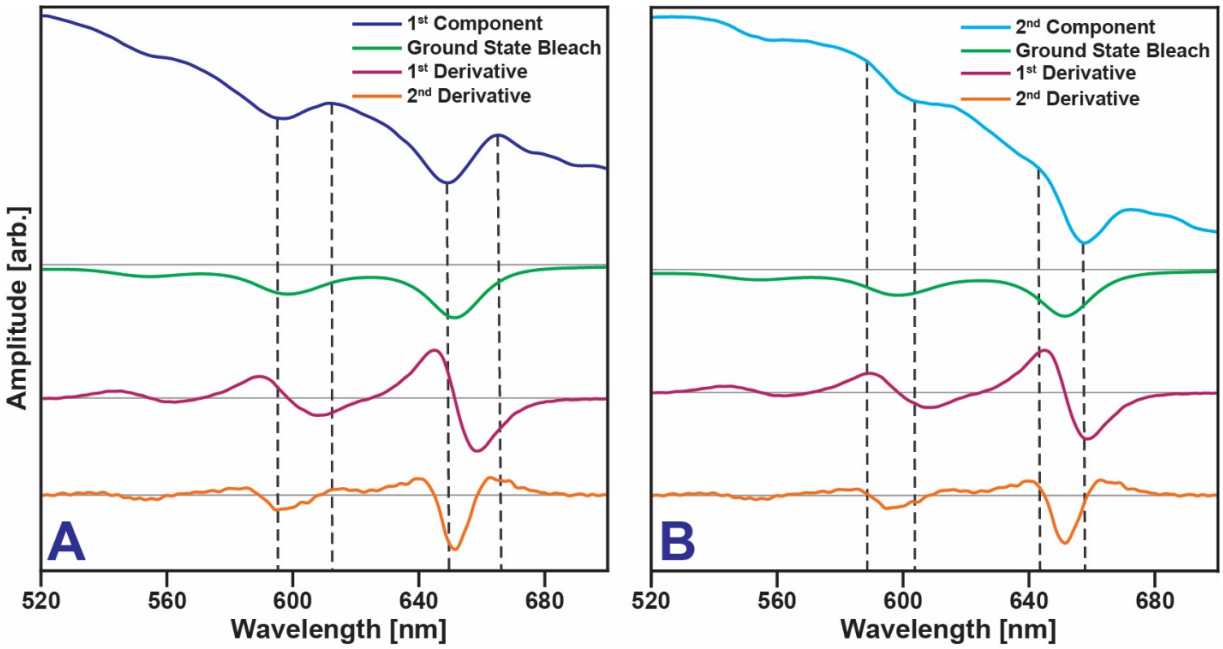

Figure S3: (A) 1st component and (B) 2nd component of our linear decomposition model compared to the ground state bleach and 1st and 2nd derivative of the 2-CP ground state absorption spectrum.

absorption lineshape and that these features gradually shift to better resemble the first derivative of 2-CP's ground state absorption before decaying altogether. In this section, we provide additional data supporting this conclusion.

In Figure S3A, we compare the first component recovered by our DADS analysis of 2-CP:PbS against 2-CP's expected ground state bleaching lineshape and the first and second derivatives of 2-CP's ground state absorption spectrum. Figure S3B does the same for the second component recovered from our DADS analysis. Guidelines are plotted in each panel to draw the eye to noteworthy features for comparison. Looking at the first component DADS in Figure S3A, the spectrum is a linear combination of PbS NC induced absorption features with 2-CP induced absorptions and bleaches superimposed. Comparing the 1st component lineshape to the spectra plotted below it, it is clear the 2-CP first derivative lineshape cannot explain the observed features due to disagreement in the position of spectral bands. Focusing on the lowest energy features, there is a photobleach at ~655 nm that matches photobleaching features expected from both the 2-CP

ground state absorption lineshape as well as its second derivative. However, there is a well-defined induced absorption in the 1st component at ~665 nm and a weaker induced absorption at ~615 nm that only appear in the second derivative spectrum, leading us to conclude the second derivative lineshape best reproduces the 2-CP features seen immediately upon photoexcitation. Turning our focus to the second DADS in Figure S3B, we see the features of the 2nd component associated with 2-CP no longer agree with either the 2-CP ground state bleach or its second derivative. Rather, they are best reproduced by the first derivative of 2-CP's ground state absorption lineshape.

To summarize, immediately upon photoexcitation, we observe features that initially resemble the second derivative of 2-CP's ground state absorption spectrum that, over 3.3 ps, evolve to better resemble the first derivative of 2-CP's ground state absorption spectrum. This latter feature then decays on a 37 ps timescale. While one potential interpretation of these two observed timescales is rapid charge transfer from PbS to 2-CP followed by charge recombination to form a surface state, it is not obvious why the intermediate charge-separated state in this scenario (Figure S3B) would display an induced absorption spectrum akin to 2-CP's first derivative rather than its cation or anion spectrum.[7] This scenario also does not explain the appearance of 2-CP's second derivative lineshape immediately upon photoexcitation. Rather, we assign the observed dynamics to Stark-induced shifts of 2-CP's ground state absorption lineshape. Upon photoexcitation, 2-CP molecules experience a dipolar field produced by the PbS NC exciton that causes the HOMO-LUMO gap of some molecules to narrow and others to widen, leading to the second derivative lineshape. Over time, as carriers localize to the NC surface, the field distribution narrows, causing 2-CP molecules to experience a more uniform field that shifts their absorption transitions in the same direction on average, producing a transient lineshape that resembles the first derivative of 2-CP's ground state absorption.

SIV. Transient Absorption Spectra of Neat PbS Nanocrystals

Within the first 50 ps following photoexcitation, TA spectra of 2-CP:PbS display the growth of a photobleach centered near 715 nm that we assign to localized carrier states at the PbS NC surface. This band decays with a 113-ns time constant concomitant with the growth of an induced absorption band centered near 540 nm we assign to 2-CP triplet excitons. To highlight that these features are not present in TA spectra of neat PbS, in Figure S4 we plot TA dynamics of neat PbS NCs suspended in toluene recorded at probe wavelengths of 540 and 715 nm. At both wavelengths, an induced absorption can be seen that decays over a few microseconds. Both traces can be fit well by a biexponential function with time constants of 0.38 and 3.0 μs (dashed black lines), although we note a single exponential decay with a decay constant of 2 μs also does an

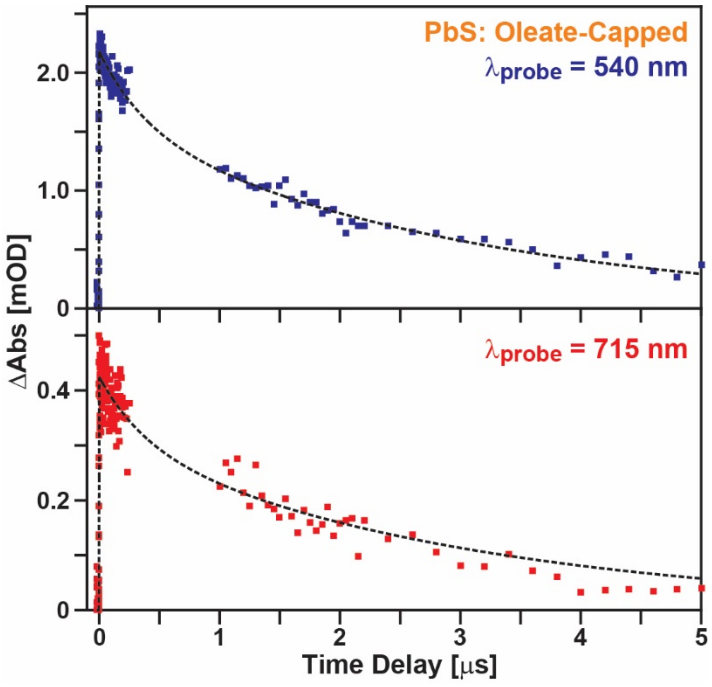

Figure S4: TA kinetics of oleate-capped PbS NCs in toluene following excitation at 1064 nm. The decay of the induced absorption observed at both 540 and 715 nm can be well fit by a biexponential function (dashed black) with time constants of 0.38 and 3.0 μs. The gap in each dataset between ~0.25 and 1 μs results from a RF-background that interferes with our detection electronics.

admirable job reproducing the observed kinetics. Since no photobleaching at 715 nm is observed nor dynamics occurring on a 113 ns timescale, the spectral changes reported for 2-CP:PbS in the main text cannot be assigned to intrinsic relaxation dynamics of PbS NCs.

SV. Transient Absorption Spectra of 2-CP:PbS for Varying Excitation Densities

As described in the main text, TA spectra of 2-CP:PbS display the growth of a new photobleaching feature centered near 710 nm. One potential assignment for this band is the formation of 2-CP excimers, which have been shown to display stimulated emission near 710 nm in prior ultrafast studies.[8] However, given the energy of a 2-CP excimer exceeds that of the 804 nm photons we use to excite 2-CP:PbS, the formation of this state would necessitate the absorption of multiple photons by a single NC. In Figure S5, we plot TA kinetic traces showing how the development of the photobleaching band at 710 nm changes as the average number of excitations per NC, $\langle N_{Ex} \rangle$, is varied. Data shown in Figures 2, 3, and 5 of the main text were recorded using a pump energy that yields a value of 1.48 for $\langle N_{Ex} \rangle$. As this value is lowered, we see no discernable changes in the dynamics governing the growth of the 710 nm photobleach. This leads us to the

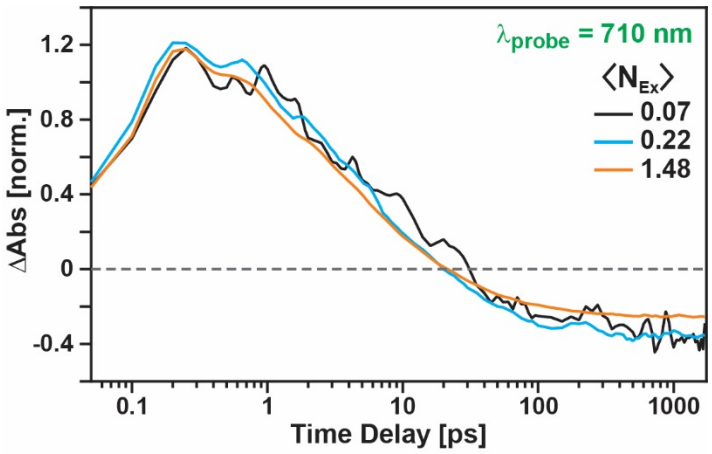

Figure S5: TA kinetics of 2-CP:PbS measured at a probe wavelength of 710 nm for different pump fluences.

conclusion that the growth of this feature is not a multiphoton effect, allowing us to rule out 2-CP excimer formation as the origin of this feature. Rather, as we argue in the main text, we assign this band to charge carrier localization at PbS surfaces.

SVI. 2-CP Triplet Sensitization

To identify spectral signatures of 2-CP triplet excitons, we prepared a dichloromethane solution containing 2-CP and platinum octaethylporphyrin (PtOEP). Photoexcitation of PtOEP forms a singlet excited state that rapidly intersystem crosses to its corresponding triplet state ($1/k_{ISC}$ = 165 fs).[6] As PtOEP's triplet energy exceeds that of 2-CP, diffusive encounter of excited PtOEP molecules and 2-CP molecules can produce 2-CP triplet excitons. Figure S6 displays TA spectra measured following PtOEP excitation. Shortly after excitation, a prominent photobleach can be seen at 535 nm that signals depletion of PtOEP's ground state. An induced absorption can also be seen to rise to the blue of these bleaching transitions that is indicative of PtOEP's lowest

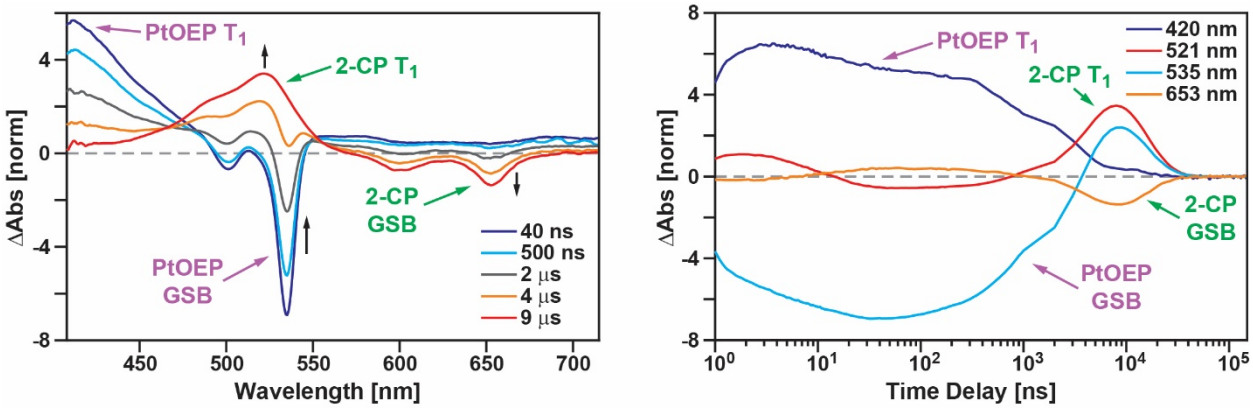

Figure S6: (Left) TA spectra of a 2-CP:PtOEP mixture measured following excitation of PtOEP at 532 nm. Over a few microseconds, features attributed to PtOEP's T_1 state and ground state bleach (GSB) deacy as bands attributed to 2-CP's T_1 state and GSB appear. (Right) Kinetic traces measured at wavelengths corresponding to PtOEP's T_1 state (420 nm, blue), 2-CP's T_1 state (521 nm, red), PtOEP's GSB (535 nm, cyan), and 2-CP's GSB (635 nm, orange). Following its creation, 2-CP's T_1 state decays with a time constant of 11.6 µs. The growth of the PtOEP GSB on nanosecond time delays reflects some overlap with an induced absorption of 2-CP's S_1 state as a small fraction of 2-CP molecules are also excited by the 532 nm pump. The majority of directly excited 2-CP molecules decay to the ground state over ~10 ns and do not contribute to the measured dynamics on microsecond timescales.

triplet excited state.[6] Over the course of a few microseconds, we observe loss of these features concomitant with the growth of photobleaching transitions centered at 600 and 652 nm that signal triplet exciton transfer to 2-CP. In addition to these features, 2-CP's triplet spectrum contains a prominent induced absorption band centered at 521 nm. This feature is similar to bands that have been assigned to triplet excitons in prior work on TIPS-pentacene and related derivatives.[7–12] Over time, we find 2-CP triplets decay with a 11.6 μs lifetime. This value is on the lower side of the range of lifetimes previously reported for TIPS-pentacene and may reflect a shortening of the lifetime from the addition of a benzoic acid functional group at TIPS-pentacene's 2 position or enhanced intersystem crossing to the ground state due to the dichloromethane solvent.

SVII. Changes in Absorption Spectra upon Treatment with Differing Amounts of 2-CP

In the main text and Section SIII above, we note spectral signatures we assign to the formation of localized charge carriers are absent from TA spectra of neat PbS NCs, insinuating sites that localize carriers are produced by the 2-CP ligand exchange process. One mechanism that may facilitate the formation of such localized states is removal of surface Pb^{2+} ions as part of a

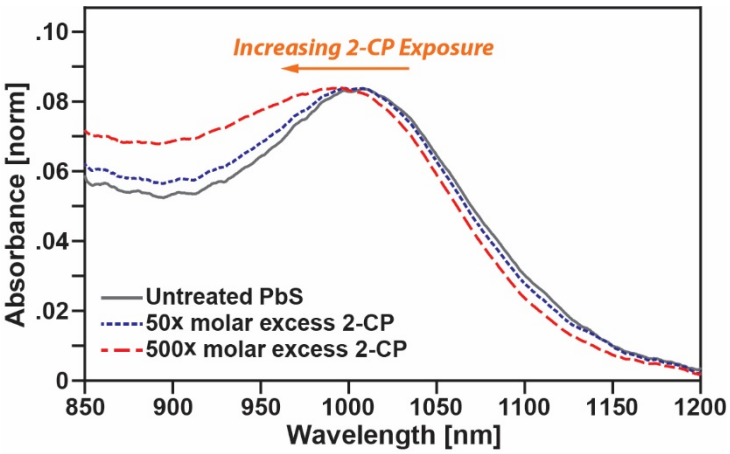

Figure S7: Absorption spectra of PbS NCs following treatment with 2-CP. Spectra have been normalized to the peak of the PbS X1 band.

coordination complex formed with leaving oleate ligands.[13] As partial support for this hypothesis, in Figure S7, we plot absorption spectra of PbS NCs that have been subjected to ligand exchange with 50 molar excess 2-CP and 500 molar excess 2-CP. Examining the position of the X1 absorption band, we find as the amount of 2-CP used to treat the NCs is increased, the X1 band displays a gradual shift towards higher energy. Given both oleate and 2-CP employ identical carboxylic acid linking groups, this shift is unlikely to be caused by a change in the electronic structure of PbS upon exchange of oleate for 2-CP. Rather, this shift suggests a slight etching of the NC surface, which would be consistent with the loss of Pb^{2+} ions during ligand exchange.

SVIII. Spin-Triplet State Identification via Constrained Density Functional Theory

We use constrained density functional theory (CDFT)[14] to locate different localized triplet states associated with 2-CP:PbS. A PbS NC is cut out from the bulk PbS structure (rock salt) using a Wulff construction polygon.[15] We decorate the PbS NC with amine ligands to model the passivation of the surface. The amine ligands are used for computational convenience rather than oleate ligands as the latter are bidentate ligands and have a variety of potential binding motifs on the surface compared with monodentate amine ligands. The amine ligands are placed at a distance of 2 Å from a surface lead atom. We replace one of the amine ligands with a 2-CP molecule at a distance of approximately 2 Å from a lead atom at the surface, following structural optimization using a 6-31G*/B3LYP DFT calculation.

In the CDFT calculations, we constrained the triplet spin to be located on the NC or the 2-CP molecule. All calculations were performed at the single molecular geometry described above. The geometry here is not necessarily representative of the range of structures probed in the experiment, but we argue qualitative electronic features will not be highly sensitive to the particular choice of NC size, doping, and surface passivation. In all the calculations, we used the

LANL2DZ basis set and effective core potentials with the PBE0 functional. Because the NC surface is defective, it is highly likely there are multiple stable triplet states for the system. Convergence to such states is generally hard, and so we use CDFT to aid in the search – we used CDFT to generate various localized triplet states (on the 2-CP molecule, in the bulk of the NC, on the surface of the NC). As expected, these calculations revealed the existence of multiple Kohn-Sham solutions, corresponding to different excited states of the complex.

Constraining the triplet spin on all the atoms in the NC results in a triplet spin-density located on the surface of the NC that is not close to the 2-CP molecule. Constraining the triplet spin on the bulk atoms of the NC following a constraint on the full NC instead yields a triplet spin density located mainly on the bulk of the NC. In contrast, constraining the triplet spin on half of the NC's atoms closer to the 2-CP molecule following a constraint on the full NC produces a triplet spin density located on the surface of the NC close to the 2-CP molecule. All three excited states in which the exciton resides on the NC have very similar energies, with a maximal energy difference of only $\Delta E \cong 37\ meV$ between then. All DFT/CDFT calculations were performed using Qchem,[16] while Vesta[17,18] was used to render images appearing in Figure 6 of the main text.

References

(1) Sanders, S. N.; Kumarasamy, E.; Pun, A. B.; Trinh, M. T.; Choi, B.; Xia, J.; Taffet, E. J.; Low, J. Z.; Miller, J. R.; Roy, X.; Zhu, X.-Y.; Steigerwald, M. L.; Sfeir, M. Y.; Campos, L. M. Quantitative Intramolecular Singlet Fission in Bipentacenes. *J. Am. Chem. Soc.* **2015**, *137* (28), 8965–8972.

(2) Shi, D.; Ren, Y.; Jiang, H.; Lu, J.; Cheng, X. A New Three-Dimensional Metal–organic Framework Constructed from 9,10-Anthracene Dibenzoate and Cd(II) as a Highly Active Heterogeneous Catalyst for Oxidation of Alkylbenzenes. *Dalton Trans* **2013**, *42* (2), 484–491.

(3) Shu, Y.; Lim, Y.-F.; Li, Z.; Purushothaman, B.; Hallani, R.; Kim, J. E.; Parkin, S. R.; Malliaras, G. G.; Anthony, J. E. A Survey of Electron-Deficient Pentacenes as Acceptors in Polymer Bulk Heterojunction Solar Cells. *Chem Sci* **2011**, *2* (2), 363–368.

(4) Vengris, M.; Horst, M. A. van der; Zgrablic, G.; Stokkum, I. H. M. van; Haacke, S.; Chergui, M.; Hellingwerf, K. J.; Grondelle, R. van; Larsen, D. S. Contrasting the Excited-State Dynamics of the Photoactive Yellow Protein Chromophore: Protein versus Solvent Environments. *Biophys. J.* **2004**, *87*, 1848–1857.

(5) Chen, X.; Larsen, D. S.; Bradforth, S. E.; van Stokkum, I. H. M. Broadband Spectral Probing Reveals Ultrafast Photochemical Branching after Ultraviolet Excitation of the Aqueous Phenolate Anion. *J. Phys. Chem. A* **2011**, *115* (16), 3807–3819.

(6) Roberts, S. T.; Schlenker, C. W.; Barlier, V.; McAnally, R. E.; Zhang, Y.; Mastron, J. N.; Thompson, M. E.; Bradforth, S. E. Observation of Triplet Exciton Formation in a Platinum-Sensitized Organic Photovoltaic Device. *J. Phys. Chem. Lett.* **2011**, *2*, 48–54.

(7) Garakyaraghi, S.; Mongin, C.; Granger, D. B.; Anthony, J. E.; Castellano, F. N. Delayed Molecular Triplet Generation from Energized Lead Sulfide Quantum Dots. *J. Phys. Chem. Lett.* **2017**, *8* (7), 1458–1463.

(8) Walker, B. J.; Musser, A. J.; Beljonne, D.; Friend, R. H. Singlet Exciton Fission in Solution. *Nat. Chem.* **2013**, *5* (12), 1019–1024.

(9) Pensack, R. D.; Tilley, A. J.; Parkin, S. R.; Lee, T. S.; Payne, M. M.; Gao, D.; Jahnke, A. A.; Oblinsky, D. G.; Li, P.-F.; Anthony, J. E.; Seferos, D. S.; Scholes, G. D. Exciton Delocalization Drives Rapid Singlet Fission in Nanoparticles of Acene Derivatives. *J. Am. Chem. Soc.* **2015**, *137* (21), 6790–6803.

(10) Grieco, C.; Doucette, G. S.; Pensack, R. D.; Payne, M. M.; Rimshaw, A.; Scholes, G. D.; Anthony, J. E.; Asbury, J. B. Dynamic Exchange During Triplet Transport in Nanocrystalline TIPS-Pentacene Films. *J. Am. Chem. Soc.* **2016**, *138* (49), 16069–16080.

(11) Wu, Y.; Liu, K.; Liu, H.; Zhang, Y.; Zhang, H.; Yao, J.; Fu, H. Impact of Intermolecular Distance on Singlet Fission in a Series of TIPS Pentacene Compounds. *J. Phys. Chem. Lett.* **2014**, *5*, 3451–3455.

(12) Musser, A. J.; Liebel, M.; Schnedermann, C.; Wende, T.; Kehoe, T. B.; Rao, A.; Kukura, P. Evidence for Conical Intersection Dynamics Mediating Ultrafast Singlet Exciton Fission. *Nat. Phys.* **2015**, *11* (4), 352–357.

(13) Anderson, N. C.; Hendricks, M. P.; Choi, J. J.; Owen, J. S. Ligand Exchange and the Stoichiometry of Metal Chalcogenide Nanocrystals: Spectroscopic Observation of Facile Metal-Carboxylate Displacement and Binding. *J. Am. Chem. Soc.* **2013**, *135* (49), 18536–18548.

(14) Wu, Q.; Van Voorhis, T. Direct Calculation of Electron Transfer Parameters through Constrained Density Functional Theory. *J. Phys. Chem. A* **2006**, *110* (29), 9212–9218.

(15) Bealing, C. R.; Baumgardner, W. J.; Choi, J. J.; Hanrath, T.; Hennig, R. G. Predicting Nanocrystal Shape through Consideration of Surface-Ligand Interactions. *ACS Nano* **2012**, *6* (3), 2118–2127.

(16) Shao, Y.; Gan, Z.; Epifanovsky, E.; Gilbert, A. T. B.; Wormit, M.; Kussmann, J.; Lange, A. W.; Behn, A.; Deng, J.; Feng, X.; Ghosh, D.; Goldey, M.; Horn, P. R.; Jacobson, L. D.; Kaliman, I.; Khaliullin, R. Z.; Kuś, T.; Landau, A.; Liu, J.; Proynov, E. I.; Rhee, Y. M.; Richard, R. M.; Rohrdanz, M. A.; Steele, R. P.; Sundstrom, E. J.; Woodcock, H. L.;

Zimmerman, P. M.; Zuev, D.; Albrecht, B.; Alguire, E.; Austin, B.; Beran, G. J. O.; Bernard, Y. A.; Berquist, E.; Brandhorst, K.; Bravaya, K. B.; Brown, S. T.; Casanova, D.; Chang, C.-M.; Chen, Y.; Chien, S. H.; Closser, K. D.; Crittenden, D. L.; Diedenhofen, M.; DiStasio, R. A.; Do, H.; Dutoi, A. D.; Edgar, R. G.; Fatehi, S.; Fusti-Molnar, L.; Ghysels, A.; Golubeva-Zadorozhnaya, A.; Gomes, J.; Hanson-Heine, M. W. D.; Harbach, P. H. P.; Hauser, A. W.; Hohenstein, E. G.; Holden, Z. C.; Jagau, T.-C.; Ji, H.; Kaduk, B.; Khistyaev, K.; Kim, J.; Kim, J.; King, R. A.; Klunzinger, P.; Kosenkov, D.; Kowalczyk, T.; Krauter, C. M.; Lao, K. U.; Laurent, A. D.; Lawler, K. V.; Levchenko, S. V.; Lin, C. Y.; Liu, F.; Livshits, E.; Lochan, R. C.; Luenser, A.; Manohar, P.; Manzer, S. F.; Mao, S.-P.; Mardirossian, N.; Marenich, A. V.; Maurer, S. A.; Mayhall, N. J.; Neuscamman, E.; Oana, C. M.; Olivares-Amaya, R.; O'Neill, D. P.; Parkhill, J. A.; Perrine, T. M.; Peverati, R.; Prociuk, A.; Rehn, D. R.; Rosta, E.; Russ, N. J.; Sharada, S. M.; Sharma, S.; Small, D. W.; Sodt, A.; Stein, T.; Stück, D.; Su, Y.-C.; Thom, A. J. W.; Tsuchimochi, T.; Vanovschi, V.; Vogt, L.; Vydrov, O.; Wang, T.; Watson, M. A.; Wenzel, J.; White, A.; Williams, C. F.; Yang, J.; Yeganeh, S.; Yost, S. R.; You, Z.-Q.; Zhang, I. Y.; Zhang, X.; Zhao, Y.; Brooks, B. R.; Chan, G. K. L.; Chipman, D. M.; Cramer, C. J.; Goddard, W. A.; Gordon, M. S.; Hehre, W. J.; Klamt, A.; Schaefer, H. F.; Schmidt, M. W.; Sherrill, C. D.; Truhlar, D. G.; Warshel, A.; Xu, X.; Aspuru-Guzik, A.; Baer, R.; Bell, A. T.; Besley, N. A.; Chai, J.-D.; Dreuw, A.; Dunietz, B. D.; Furlani, T. R.; Gwaltney, S. R.; Hsu, C.-P.; Jung, Y.; Kong, J.; Lambrecht, D. S.; Liang, W.; Ochsenfeld, C.; Rassolov, V. A.; Slipchenko, L. V.; Subotnik, J. E.; Van Voorhis, T.; Herbert, J. M.; Krylov, A. I.; Gill, P. M. W.; and Head-Gordon, M. Advances in Molecular Quantum Chemistry Contained in the Q-Chem 4 Program Package. *Mol. Phys.* **2015**, *113* (2), 184–215.

(17) Humphrey, W.; Dalke, A.; Schulten, K. VMD: Visual Molecular Dynamics. *J. Mol. Graph.* **1996**, *14*, 33–38.

(18) Momma, K.; Izumi, F. VESTA3 for Three-Dimensional Visualization of Crystal, Volumetric and Morphology Data. *J. Appl. Crystallogr.* **2011**, *44* (6), 1272–1276.